scientific reports

Check for updates

OPEN

Biochar structure development during slow pyrolysis of pellets from barley straw and bran

Maryna Zhylina[1,2], Denis Miroshnichenko[3,4]✉, Andrii Melnykov[5], Valentina Stepanova[1], Kristine Lazdovica[6], Vjaceslavs Zemcenkovs[7], Vita Sterna[2] & Jurijs Ozolins[1]

In recent years, there has been a significant drive to incorporate circularity into products by finding cost-effective methods to recycle and reuse industrial waste. Agricultural biomass, a widespread waste stream, has great potential as a raw material for producing sorbents. However, the common practice of waste incineration negates this opportunity, as valuable resources are lost. This study aims to demonstrate that biomass pyrolysis can be used to create value-added products such as sorbents. Prior to pyrolysis, the optimal granulation process for integrating barley straw with bran was determined, yielding durable pellets composed of 90% barley straw and 10% bran (BSB). The study comparatively analyzed biochar obtained from BSB pellets, which were first pelletized and then subjected to pyrolysis at different temperatures (600, 700, and 800 °C) and holding times (1, 2, and 3 h). Key properties examined included biochar yield, carbon and nitrogen content, specific surface area, pore size distribution, and BET surface area. Pyrolysis was carried out at a constant heating rate of 5 °C·min^{-1}. Increasing the holding time and pyrolysis temperature positively influenced the surface area and broadened the pore size distribution of the resulting biochar. The most favorable results were observed for the sample obtained at 800 °C. The total pore volume of samples BSB800-2 h and BSB800-3 h was notably higher than that of BSB800-1 h. Prolonged holding time at the final temperature led to an expansion in pore size range and a corresponding increase in total pore volume and surface area.

Keywords Biomass, Granulation, Pyrolysis, Biochar, Surface area, Pore distribution

The European Commission has demonstrated a strong commitment to transitioning towards a circular economy, with significant efforts in this direction beginning in 2015. Its sustainability strategy emphasizes key areas such as reducing emissions from transportation, advancing renewable energy, promoting organic farming, and enhancing the recycling of various waste streams. Progress in recycling research is enabling more efficient interventions to achieve climate-friendly outcomes[1]. Agricultural activities in the EU generate approximately 1.466 million tons of dry biomass waste annually. This waste is often incinerated, but as biomass is both biodegradable and renewable, it holds the potential to be converted into biochar, sorbents, and heating briquettes[2]. Recent advances in biomass valorization increasingly focus on pelletized and pyrolyzed materials as efficient and sustainable alternatives for environmental remediation and material recovery. For instance, the work by Vincevica-Gaile et al.[3] highlights the potential of converting various industrial residues, including wood ash and coffee grounds, into biochar pellets via low-temperature pyrolysis, demonstrating promising sorption characteristics for wastewater treatment and soil improvement. Similarly, composite sorbents developed from peat, rubber, and cenospheres have shown effective oil product adsorption, emphasizing the relevance of bio-based granules in pollution control applications[4]. The growing interest in sorptive materials derived from waste is further supported by studies on cenospheres from fly ash for syntactic foam development[5] and on waste glass

[1]Faculty of Natural Sciences and Technology, Institute of Biomaterials and Bioengineering, Riga Technical University, Paula Valdena Street 3, K-1, Riga 1048, Latvia. [2]Institute of Agricultural Resources and Economics, Stende Research Centre, Dizzemes, Dizstende, Libagu Parish, Talsu County 3258, Latvia. [3]Department of Oil, Gas and Solid Fuel Processing Technology, National Technical University Kharkiv Polytechnic Institute, 2, Kyrpychova str, Kharkiv 61002, Ukraine. [4]Coal Department, State Enterprise Ukrainian State Research Institute for Carbochemistry (UKHIN), Kharkiv 61023, Ukraine. [5]Scientific Research Institution "Ukrainian Scientific Research Institute of Ecological Problems (USRIEP)", 6, Evgeniya Yenin Str, Kharkiv 61166, Ukraine. [6]Institute of Chemistry and Chemical Technology, Faculty of Science and Technology, Riga Technical University, Paula Valdena St, 3/7, Riga 1048, Latvia. [7]Institute of Materials and Surface Engineering, Faculty of Natural Sciences and Technology, Riga Technical University, 7, P, Valdena Str, Riga 1048, Latvia. ✉email: Denys.Miroshnychenko@khpi.edu.ua

integration into ceramic foams for efficient dye removal from industrial effluents[6]. Notably, spent coffee grounds (SCG) have been studied as a rich source of extractable bioactive compounds, with their valorization aligning with biorefinery strategies that emphasize multiproduct recovery from biomass streams[7]. Additionally, activated carbon prepared from industrial sludge[8] and heat-treated diatomite[9] has demonstrated strong potential for the adsorption of synthetic dyes, confirming the relevance of structural tuning through thermal or chemical treatment. These studies collectively underscore the potential of diverse residual biomass sources and post-consumer materials for producing functional sorbents, supporting the transition to a circular economy and biorefinery-based waste management paradigm.

The valorization of biomass can be realised through pyrolysis, with thermal analysis indicating that low-temperature slow pyrolysis yields high-quality products. The affordability of these products is attributed to the use of plant waste as a raw material, the relatively low energy requirements of the process, and the reduced need for waste disposal. Lignocellulosic biomass, a widely available and cost-effective carbon source, is gaining significant attention as a precursor for various carbon-based materials. Its renewability, environmental sustainability, and accessibility make it an appealing option, Biomass serves as a renewable resource capable of providing clean and affordable energy. These benefits position biomass as a sustainable alternative to fossil fuels, supporting the management of forestry and lignocellulosic residues to produce chemicals, biofuels, and carbon materials[10]. Each region has its own plant waste that requires disposal, so different types of plant residues appear in publications, from walnut shells[11], citrus seeds[12] to cane[13] and wheat straw[14]. (Table 1) provides an overview of various raw materials, the technologies employed to produce different products and their properties. Pyrolysis operates within a temperature range of 200 °C to 850 °C. When biochar is intended for use as a sorbent, an activation process is often employed to enhance its surface area. Chemical activation involves using substances like $ZnCl_2$, HNO_3, K_2CO_3, and HCl, Additionally, the curing time in the furnace, which can range from 0.5 to 6 h, influences the resulting surface area.

Although the production of biochar from biomass via pyrolysis has been extensively studied, most of the existing research employs unprocessed feedstocks and often neglects pre-treatment methods such as granulation, which can significantly influence thermal behavior, devolatilization dynamics, and pore structure development. The impact of biomass compaction prior to pyrolysis on the formation of porous carbon frameworks - particularly its effects on heat transfer, volatile release, and structural evolution remains insufficiently explored in current literature[3,22]. Existing biochar materials derived from powdery biomass typically suffer from low mechanical stability and limited applicability in packed-bed or dynamic sorption systems.

This study aims to address this research gap by investigating the structural transformation of biochar obtained from mechanically compacted agricultural residues. Barley straw and bran were granulated into uniform pellets and subjected to controlled slow pyrolysis at different temperatures and residence times. The choice of granule composition – 90% barley straw and 10% barley bran (BSB) - was guided by the need to ensure both structural integrity during granulation and thermal stability during pyrolysis as well it follows from previous works[3]. Barley

Feedstock	Pyrolysis temp, °C	Yield wt %	t, h	Heat. rate, °C·min^{-1}	Activat	Total pore volume cm^3·g^{-1}	S_{BET}, m^2·g^{-1}	Ref.
Corn stover	60–600	-	-	-	-	-	293–527	15
Walnut shell	400	-	1	10	-	0.078	74.06	11
Walnut shell	500	-	1	10	-	0.150	128.52	
Walnut shell	600	-	1	10	-	0.296	488.89	
Walnut shell	700	-	1	10	-	0.695	737.98	
Peanut shell	600	-	0.5	-	K_2CO_3	0.211	502.23	16
Peanut shell	600	-	0.5	-	K_2CO_3	0.320	750.16	
Peanut shell	600	-	0.5	-	K_2CO_3	0.433	1087.92	
Pine sawdust	850	10.01	1	5	KOH	1.46	2864.5	17
Pine sawdust	600	14.6	1	5	KOH	1.09	2437,2	
Pine sawdust	850	19.3	1	5	$ZnCl_2$	0.26	471.4	
Rapeseed husk	200	47.14	0.5	5	-	-	-	18
Orange peel	200	61.60	6	-	HCl	0.010	7.75	19
Orange peel	400	30.00	6	-	HCl	0.010	42.4	
Orange peel	700	22.20	6	-	HCl	0.035	201	
Wheat straw	450	-	4	10	-	0.048	45.05	20
Wheat straw	550	-	4	10	-	0,294	140.54	
Wheat straw	650	-	4	10	-	0.333	110.87	
Wheat straw	750	-	4	10	-	0.306	139.78	
Wheat straw	850	-	4	10	-	0.259	158.42	
Food waste	600	30.9	4	5	-	-	1.36	21
Food waste + wooden sawdust	600	35.4	4	5	-	-	1.83	
Min	60	10.01	0.5	5	-	0.01	1.36	-
Max	850	61.6	6	10	-	1.46	2864.5	-

Table 1. Characteristics of Raw materials and pyrolysis modes for obtaining sorbents from plant residues.

bran functioned as a sustainable binder, improving the mechanical stability of pellets without introducing chemical additives that could affect the thermal decomposition behavior. The selected ratio was optimized experimentally to balance pellet strength feedstock homogeneity and porosity development in the final biochar. The objective is to evaluate how compaction and thermal treatment influence the surface area, pore size distribution, and carbon content of the resulting biochar. The approach contributes to the development of robust sorbent granules and supports EU strategies for biorefinery development and circular bioeconomy[3]. Unlike previous studies that primarily used raw or loose biomass, this study investigates the effects of pre-pelletization on biochar structure, highlighting the role of compaction in pore development and thermal behavior.

These biochar pellets are considered as precursors for sorbent materials aimed at wastewater purification and environmental remediation. The present study focuses on understanding how slow pyrolysis parameters affect key structural features such as specific surface area, porosity, and surface functionality, which are essential for adsorption efficiency. In further work, these biochars will be steam-activated and evaluated as sorbents for the removal of organic contaminants and heavy metals from municipal and agricultural wastewater, supporting their application in environmental remediation.

The innovation of this research lies in the use of wet granulation techniques to form plant-residue-based precursors into mechanically robust granules prior to carbonization. Traditional methods using powdery biomass often result in carbon materials that are fragile, have low bulk density, and are prone to attrition, making them less suitable for continuous-flow applications such as packed-bed columns or filtration systems[23,24]. In contrast, the granulation approach – particularly wet granulation using a pelletizer - offers a scalable and binder-free pathway to create structured precursors that retain their geometry and mechanical integrity after thermal treatment. This method enhances the structural strength and stability of the final carbon framework, leading to improved handling, reduced pressure drop in flow systems, and enhanced reusability[25,26]. Furthermore, by avoiding the use of binders (bran), the process remains chemically clean and sustainable. Despite these advantages, relatively few studies have explored the direct transformation of bio-based granules into functional carbon sorbents, representing a gap in the literature that this work aims to address[27].

Materials and methods

This study used barley straw (BS) and barley bran (B) as feedstock to fully evaluate the potential of biochar production. BS and B were selected because they are abundant, low-cost European residues that enable valorization without competing with food/feed; BSB lignocellulosic profile (high cellulose/hemicellulose, moderate lignin) favors stable carbon formation during pyrolysis; and B complements BS with polysaccharides and phenolics, aiding densification and adding value to milling by-products[28,29]. Barley bran diluted with 70 °C hot water at a ratio of 1:1 by volume was used as a binder for straw granulation. Barley straw was taken from the fields of the research center in Stende, Talsu District, Latvia, barley bran was obtained from the same research center from the harvested crop.

The proximate composition of the non-pyrolyzed barley straw–bran pellets was determined following standard procedures. Moisture content was measured by oven drying at 105 ± 2 °C in a UF 110 (Memmert GmbH Co. KG, Germany) to constant weight (ISO 18134-3:2015). Volatile matter, fixed carbon, and ash content of the solid samples were determined according to EN 14918:2010; ISO 562:2010; DIN 51749:2016; EN 14775:2009 standards, respectively. All analyses were performed in duplicate and expressed as average values. All values are reported on a dry basis (d.b.).

Pyrolysis conditions were carefully selected to investigate how thermal treatment parameters influence the microstructural evolution of biochar derived from compacted biomass. A heating rate of 5 °C·min^{-1} was applied to allow gradual devolatilization and to reduce the risk of structural collapse, which is considered particularly relevant for pre-compacted materials. Final temperatures of 600 °C (BSB600), 700 °C (BSB700), and 800 °C (BSB800), along with holding times of 1, 2, and 3 h, were chosen to systematically explore the effects of temperature and residence time on carbon content, pore development, and surface area. It is hypothesized - based on existing literature - that higher temperatures may enhance pore formation and increase surface area due to more intense devolatilization, while extended holding times could facilitate further rearrangement of the carbon matrix, potentially leading to a more developed microporous structure.

The raw materials were initially pre-crushed using a VIKING GE 250 S (Viking GmbH, Kufstein, Germany) followed by a second grinding stage with a disintegrator. Analysis of the granulometric composition indicated that the degree of grinding on the Veb Nosser Maschinenbau 8255 disintegrator (Nossen, Germany) did not influence the characteristics or percentage distribution of the resulting fractions what was investigated in the previous study[30]. The entire biochar production process includes 3 key stages: preparation of raw materials; formation of a homogeneous wet mixture; granulation.

The extrusion pelletizing machine ZLSP 20.OB (Anyang Best Complete Machinery Engineering Co., Ltd., China), equipped with a die plate of 310 mm internal diameter and 6 mm die holes, was used for granulation in this study. The structural description of this pelletizing unit, comprising a set of rollers and a perforated die plate, is based on technical specifications provided by the manufacturer and previous literature[31]. In this configuration, the material designated for pelletization is fed into a chamber located above the roller–die system, allowing for uniform distribution. During operation, the rollers apply pressure to compress the feedstock through the die openings, forming cylindrical extrudates. These are subsequently cut into uniform pellets by an integrated cutting mechanism. Although the technical design suggests that the combination of compression, mechanical force, and precision cutting ensures consistent pellet formation, it should be noted that these operational parameters were not specifically investigated in the present study. For optimal mechanical strength what was investigated in the previous study[30], a composition of 90% pant material (barley straw) and 10% ban was selected for further experimentation.

Pellet quality assessment

For each batch, ≥ 100 pellets were inspected. The proportion of intact pellets (%) was calculated according to Eq. (1):

$$Int.\,(\%) = \frac{N_{un}}{N_{total}} \times\ 100 \tag{1}$$

where N_{un} is the number of undamaged pellets, N_{total} is the total number of pellets counted during the analysis. Length (mm) was measured with a digital calliper (resolution 0.01 mm) on 30 randomly selected pellets per batch. Visible microcracks were recorded by stereomicroscopy (≥ 10×).

The raw materials were analyzed using thermogravimetric analysis (TGA) and differential scanning calorimetry (DSC) on a STA 449 F5 Jupiter (Netzsch, Germany) and a synchronous thermoanalyzer to study the biomass pyrolysis process. The analysis parameters included a sample weight 60 mg, a heating rate of 5 °C·min^{-1}, and a temperature range of 28 to 900 °C. The experiments were conducted under an inert nitrogen atmosphere with a flow rate of 20 ml·min^{-1}. These analyses were conducted to optimize the pyrolysis process parameters.

The pyrolysis of raw materials was performed in a metal pyrolyser (chamber 150 × 210 × 130 mm) with an inert argon gas supply, allowing for the removal of volatile compounds. The pyrolyser filled with granules was placed in an LE 05111 muffle furnace (LAC, Czech Republic) and heated in an argon atmosphere to a temperature range of 500–800 °C at a heating rate of 5 °C·min^{-1} (slow pyrolysis). The inert gas flow rate was maintained at 20 ml·min^{-1} with the final temperature held from 1 to 3 h. The yield of the final product was calculated according to Eq. (2):

$$Y\,(\%) = \frac{m_2}{m_1} \times\ 100 \tag{2}$$

where: $m_1$is the mass of raw material (g); m_2 is the mass of biochar (solid residue) after pyrolysis (g).

Carbon and nitrogen contents were determined on an elemental analyser Fleshsmart NC Soil (GmbH, Germany).

Before the experiment the surface of the pellets undergoes a degassing process to remove any adsorbed contaminants and residual gases ensuring a clean and uncontaminated surface for accurate analysis. Degasification is performed to eliminate moisture and other impurities adsorbed from the air on sample surfaces. An Autosorb Degasser Model AD-9 was used for degassing, and 9 mm round sample cells were selected. Sample weights ranged from approximately 0.35 to 2 g with degassing times of either 24 h at 23 °C or 3 h at 200 °C under a vacuum of approximately − 0.5 torr as recommended by IUPAC to minimize moisture content and sample loss during degassing. After degasification the samples were reweighed. The samples' specific surface area and pore structure were analyzed using the Quadrasorb EVO gas sorption system through low-temperature nitrogen adsorption-desorption isotherms at 77 K. Pearson's product moment correlation coefficient is denoted as r for sample statistics. For a correlation between variables x and y, the formula for calculating the sample Pearson's correlation coefficient was calculated according to Eq. (3):

$$r = \frac{\sum_{i=1}^{n}(x_i - x)(y_i - y)}{\sqrt{\sum_{i=1}^{n}(x_i - x)\sum_{i=1}^{n}(y_i - y)}} \tag{3}$$

where x_i and y_i are the values of x and y for the ith individual.

A Tescan VEGA\LMS scanning electron microscope (Tescan, Brno, Czech Republic) was employed to examine the surface morphology of the granules and the fracture surface characteristics. Secondary electrons, generated at an acceleration voltage of 5 kV, were utilized for imaging. For microscopy, the samples were mounted on standard aluminum pin stubs using electrically conductive double-sided adhesive carbon tape.

3D response-surface plotting. The response surfaces shown in Fig. 8 (total pore volume, cm^3·g^{-1}, and BET surface area, m^2·g^{-1}, as functions of final temperature, °C, and holding time, min) were generated in STATISTICA 10 (StatSoft, Tulsa, USA). Experimental data points obtained from pyrolysis runs were used to fit a continuous surface by Distance-Weighted Least Squares (DWLS) interpolation (inverse-distance local least-squares smoothing). The surface was evaluated on a regular grid defined by the observed factor ranges; no extrapolation beyond the data domain was allowed. Only the fitted surface is displayed for clarity; the same axis limits and color scale were applied for both panels.

Results and discussions

Proximate composition of raw pellets

The goal was to maximise biomass content (70–95% by mass). Pellet quality was assessed by the proportion of intact pellets, mean pellet length, and the presence of visible microcracks. Increasing the bran binder from 5 wt % to 10 wt % markedly improved integrity: the share of intact pellets rose from 77% to 98%, the mean length increased from 7 mm to 10 mm, and visible microcracks were no longer observed (Fig. 1).

The proximate composition of the non-pyrolyzed barley straw–bran pellets is presented in (Table 2). The pellets exhibited a low moisture content (3.5 ± 0.3 wt %, d.b.), indicating that the material was well dried prior to thermal treatment. The volatile matter fraction (70.49 ± 1.5 wt %, d.b.) was high, which is typical for lignocellulosic agricultural residues and suggests good reactivity during pyrolysis. The fixed carbon content (18.00 ± 1.0 wt %, d.b.) is within the range reported for cereal straw-based feedstocks and provides sufficient carbon yield for further activation and sorbent production. The ash content (8.01 ± 0.5 wt %, d.b.) was slightly higher than that usually observed in pure barley straw (≈ 4–7%), which can be attributed to the inclusion of

Formulation	Intact pellets, %	Mean length, mm	Visible microcracks
95% barley straw + 5% bran	77	7	present
90% barley straw + 10% bran	98	10	absent

Fig. 1. Visual appearance and basic quality metrics of non-pyrolyzed pellets.

Non-pyrolyzed pellets	Moisture (wt%, d.b.)	Ash (wt%, d.b.)	Volatile matter (wt%, d.b.)	Fixed carbon (wt%, d.b.)
BSB (90% barley straw + 10% bran)	3.5 ± 0.3	8.01 ± 0.5	70.49 ± 1.5	18.00 ± 1.0

Table 2. Proximate composition of the non-pyrolyzed barley straw–bran pellets.

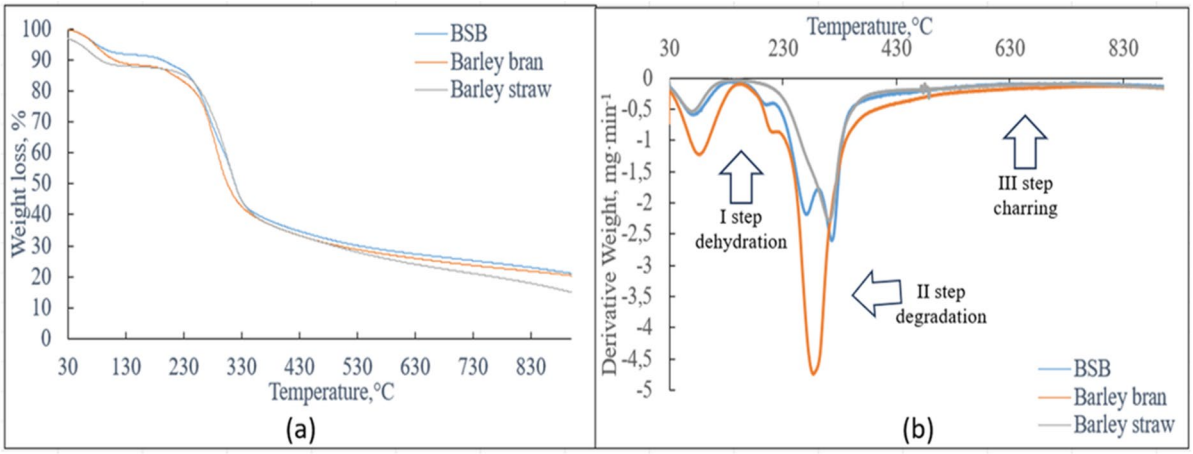

Fig. 2. Thermogravimetric analysis (TGA) results of BSB: (**a**) TG and (**b**) DTG profiles of barley straw and bran pellets.

barley bran as a binder. Such composition is favorable for subsequent slow pyrolysis, as the high volatile fraction promotes devolatilization and pore formation, while the moderate fixed carbon content ensures an adequate solid yield for further steam activation[32,33].

Carbon yield and elemental composition

The thermogravimetric (TG) and derivative thermogravimetric (DTG) curves BSB, barley straw and barley bran from 30 to 900 °C at the heating rate of 5 °C·min^{-1} are presented (Fig. 2).

The thermal degradation of BSB (Fig. 2) occurred in three significant weight loss steps: (I) dehydration, (II) degradation of components, and (III) charring of the residue. The first weight loss step, which corresponds to removing moisture and light components, occurred at the temperature range between 30 and 130 °C. The primary weight loss step happened over a wide range of temperatures from 130 to 430 °C and is related to the degradation of components of BSB. This step's inflection points (where the weight loss rate is maximum) were 257, 284 and 312 °C. The first and second inflection points are related to the degradation of hemicellulose, cellulose, starch, lignin, and protein components of barley bran. In contrast, the third point is related to the degradation of barley

Sample	Composition	Heating rate. °C·min^{-1}	Final temperature. °C	Holding time. h
BSB600-1 h	90% barley straw + 10% barley bran	5	600	1
BSB600-2 h	90% barley straw + 10% barley bran	5	600	2
BSB600-3 h	90% barley straw + 10% barley bran	5	600	3
BSB700-1 h	90% barley straw + 10% barley bran	5	700	1
BSB700-2 h	90% barley straw + 10% barley bran	5	700	2
BSB700-3 h	90% barley straw + 10% barley bran	5	700	3
BSB800-1 h	90% barley straw + 10% barley bran	5	800	1
BSB800-2 h	90% barley straw + 10% barley bran	5	800	2
BSB800-3 h	90% barley straw + 10% barley bran	5	800	3

Table 3. The composition of the pellets and the characteristics of the pyrolysis process.

Sample	Yield (after carbonization), wt %	C, wt %	*N*, wt %
BSB600-1 h	34.01 ± 0.72	51.26 ± 1.25	0.55 ± 0.05
BSB600-2 h	33.55 ± 0.58	51.47 ± 1.19	0.58 ± 0.05
BSB600-3 h	33.00 ± 0.74	50.40 ± 1.21	0.68 ± 0.04
BSB700-1 h	30.78 ± 0.71	50.65 ± 1.23	0.43 ± 0.03
BSB700-2 h	31.31 ± 0.59	47.55 ± 1.18	0.42 ± 0.03
BSB700-3 h	31.30 ± 0.67	54.48 ± 1.28	0.48 ± 0.04
BSB800-1 h	30.50 ± 0.69	47.77 ± 1.23	0.44 ± 0.03
BSB800-2 h	30.20 ± 0.82	48.10 ± 1.18	0.24 ± 0.05
BSB800-3 h	30.08 ± 0.65	46.36 ± 1.22	0.28 ± 0.05

Table 4. Yields and elemental composition of pyrolyzed pellets.

straw. The decomposition of hemicellulose (200–350 °C) starts before the decomposition of cellulose and starch (300–450 °C), but the decomposition of lignin and protein occurs over a wide temperature range between 250 and 900 °C. This step can be ascribed to the series of reactions involving dehydration, decarboxylation, and decarbonylation, and deamination, deamidation, fragmentation, and rearrangement[34]. The final weight loss step observed at the temperature range from 430 to 900 °C corresponds to the pyrolysis of lignin and charring of the residue.

Biomass-based activated carbon materials, with high specific surface area (BET). Controlled pore structure and low cost. Can effectively compete with other carbon materials that require complex and costly production methods[35]. When producing high-performance porous carbon materials. Pyrolysis technologies offer advantages in scalability and the ability to adjust process parameters to achieve desired properties in the final product. The composition of the granules and the characteristics of the pyrolysis process are provided in (Table 3). In this work biomass pellets of the same composition were carbonized at temperatures of 600, 700, and 800 °C and holding times of 1, 2, and 3 h. Biochar yield and C, N content are shown in (Table 4).

Porosity and surface area development

The adsorption isotherm (Fig. 3) illustrates the relationship between the amount of substance adsorbed and its partial pressure in the gas phase at a constant temperature of 77 K. This isotherm was measured at 31 points with the desorption curve measured at 43 points. Sorbent characteristics like specific surface area, micro- and mesopore volumes, pore diameter, and total pore volume values were determined by various methods: Brunauer–Emmett–Teller (BET), Langmuir, Barrett-Joyner-Halenda (BJH), Dollimore-Heal (DH), t-method, Dubinin-Radushkevich (DR), Density Functional Theory (DFT).

According to the IUPAC classification[36] all adsorption isotherms obtained in this study correspond to type IV, which are characterized by the presence of hysteresis loops, indicating mesoporous structures. Which is linked to capillary condensation within mesopores, and by a limitation in adsorption capacity at high relative pressures (P/P_0). The initial region of a type IV isotherm corresponds to monolayer-multilayer adsorption, mirroring the behavior observed in the analogous region of a type II isotherm for the same adsorbent in a nonporous form. These isotherms are commonly associated with numerous mesoporous industrial adsorbents. Hysteresis observed in the multilayer region of physisorption isotherms is typically attributed to capillary condensation within mesoporous structures. These hysteresis loops can display a wide range of shapes, from vertical and parallel branches in distinct gas adsorption regions to nearly horizontal and parallel branches over a broad range of relative pressures (P/P_0). Types H2 and H3 are considered intermediate forms between two extremes. A common characteristic of many hysteresis loops is the steep section of the desorption branch leading to the lower closure point. Which occurs at a relative pressure that is largely independent of the porous adsorbent's nature but primarily influenced by the adsorptive. For example, this pressure corresponds to P/P0 ≈ 0.42 in

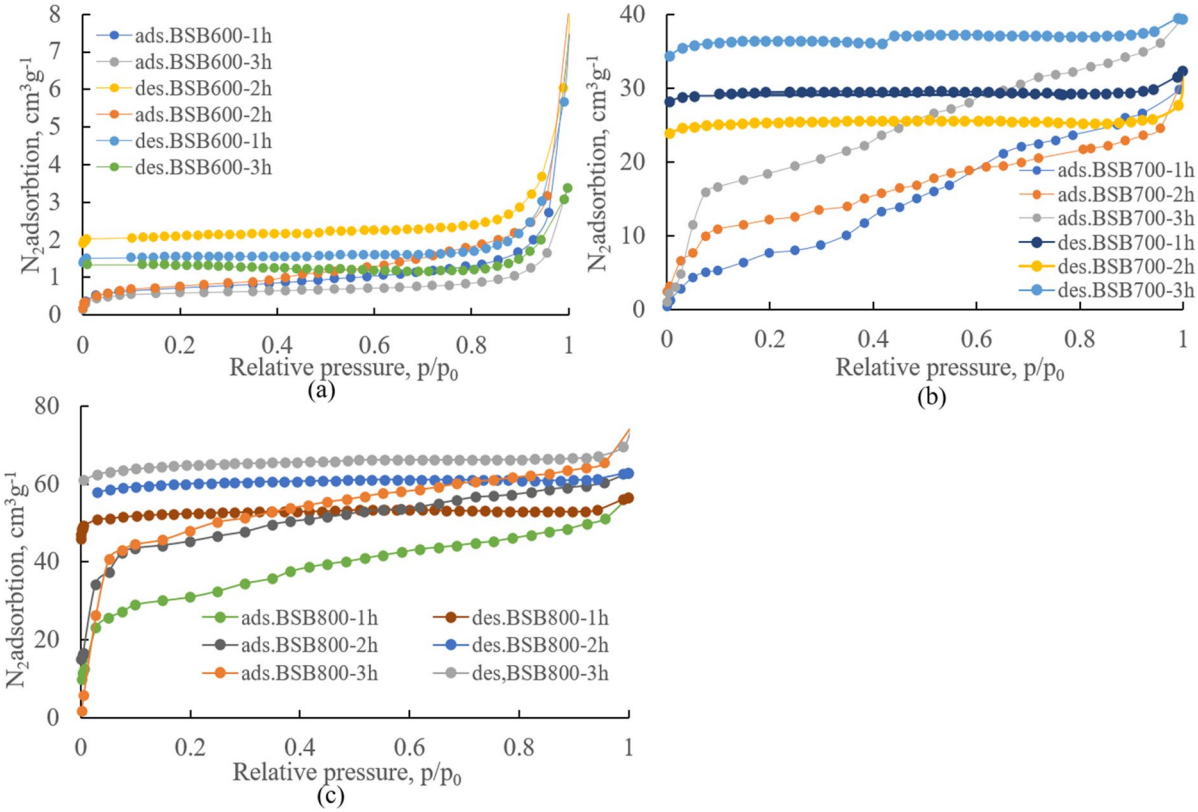

Fig. 3. N_2 adsorption-desorption isotherms for specimen pyrolyzed at 600 (**a**), 700 (**b**) and 800 °C (**c**).

nitrogen at its boiling point. According to the classification of adsorption hysteresis types. The BSB600 sample is categorized as H3, the BSB700 sample as H2, and the BSB800 sample as H4.

Based on the shape of the nitrogen adsorption isotherms. All samples are classified as micro- and mesoporous materials with specific surface areas from 2.4 to 157 $m^2 \cdot g^{-1}$ (Fig. 4).

Despite belonging to the same type. The adsorption isotherms of samples BSB600 exhibit a different slope compared to those of samples BSB700 and BSB800, suggesting differences in their pore size distribution. Sample BSB600-2 h demonstrated a pore size range of 1.5 nm to 3.00–3.25 nm. Extending the exposure time at the final heating temperature widened the pore size distribution, starting from 1.20 nm, as evidenced by the data for sample BSB600-3 h. Nonetheless, the total pore volume across the three samples showed no significant variation but sample BSB700-3 h exhibited substantial differences.

Extending the exposure time at the final temperature to 3 h resulted in a threefold increase in total pore volume and a broadened pore size range, lowering the lower limit from 1.5 nm to ~ 1 nm (Fig. 4). This is attributed to enhanced devolatilization and secondary cracking of tar residues, which open blocked channels and promote the formation of additional micro- and mesopores. Similar effects of prolonged thermal treatment on pore volume and pore widening have been previously demonstrated in studies by Belhachemi et al. [37] and Guo et al. [38]. For samples prepared at a final heating temperature of 800 °C, the pore size range remains unaffected by variations in exposure time. However, the total pore volume of samples BSB800-2 h and BSB800-3 h is notably higher than that of sample BSB800-1 h. Increasing the holding time at the final temperature leads to an expansion in the pore size range and a corresponding increase in total pore volume and surface area.

Correlation coefficient ($r > 0.9$) was used for searching strong relationship between measured characteristics (Table 5). On this basis we conclude that the results of the BET study of the surface area are in good agreement with each other, with a general increase in the surface area depending on the temperature. The dependencies of SinglePoint BET and MultiPoint BET on the final temperature are characterized by a high correlation coefficient, with values of 0.9416 and 0.9439, respectively (Fig. 5 (a)). The estimate of the surface area based on the Langmuir isotherm calculation is higher, since multilayer adsorption is not considered. The correlation coefficient between the Langmuir isotherm surface area and the final temperature is 0.9352 (Fig. 5 (a)). Given that the shape of the isotherm shows hysteresis, the values of the surface area for adsorption and desorption (BJH and DH methods) differ, and with increasing temperature, this difference becomes more significant and reaches 98.6% of the initial area BSB700-1 h. The surface area according to the adsorption isotherm calculated by the BJH and DH methods is independent of temperature for samples with a final temperature of 700 and 800 °C and is significantly lower than the results obtained by the BET method. The surface area according to the desorption isotherm is much smaller, with higher values observed at 700 °C with a holding time of 3 h and 800 °C. The value of the external pore area by the t-method correlates well with the final temperature ($r = 0.9862$) (a), and an increase in micropores by the t-method is observed along with an increase in temperature and time. There is also an increase in the area

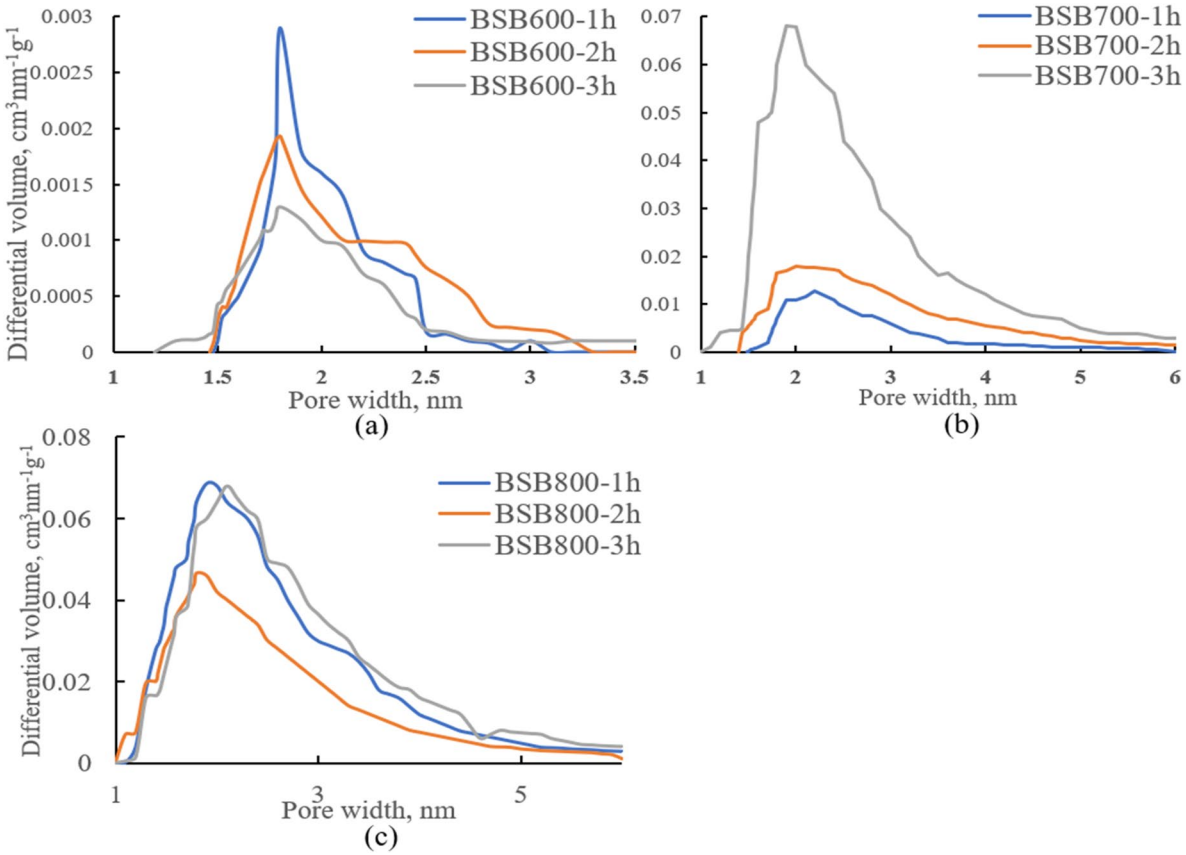

Fig. 4. Pore size distribution in the range 1–6 nm (**a**) BSB600, (**b**) BSB700, (**c**) BSB800.

Surface area calculation method, $m^2 \cdot g^{-1}$								
Sample	Single Point BET	Multi Point BET	Langmuir	BJH ads / des	DH ads / des	t-method external\ micropore	DR (micro)	DFT
BSB600-1 h	2.41	2.45	3.576	1.188/0.7607	1.23/0.7719	0.8687/1.578	5.863	4.752
BSB600-2 h	2.59	2.65	3.886	2.053/0.8519	2.169/0.8983	1.437/1.214	7.013	6.206
BSB600-3 h	1.89	1.90	2.801	0.5508/0.3855	0.5545/0.3914	0.02512/1.88	4.57	5.719
BSB700-1 h	26.6	29.1	46.8	34.59/0.4741	35.14/0.5432	22.82/6.264	94.61	88.9
BSB700-2 h	41.4	42.6	62.92	20.18/0.7253	20.61/0.9858	20.14/22.46	97.00	75.09
BSB700-3 h	62.3	64.39	111.6	27.75/4.934	28.17/5.084	26.34/38.05	153.4	107.0
BSB800-1 h	105.3	104.9	155.4	29.29/2.316	29.77/2.581	38.53/66.38	209.7	285.1
BSB800-2 h	145.8	145.5	215.8	19.12/2.528	19.39/2.702	37.51/108.0	269.8	143.0
BSB800-3 h	156.6	157.3	250.9	22.62/3.616	23.19/3.996	45.02/112.3	423.7	238.5

Table 5. Surface area and porosity characteristics of pyrolyzed pellets based on different analytical methods.

by the DR and DFT methods with increasing temperature and retention time. The results obtained indicate the intensive formation of internal branched micro- and meso-porous structures because of pyrolysis at 700 °C, and especially at 800 °C, in which capillary condensation can occur, resulting in a significant difference between the area calculated by adsorption and desorption.

The results for the total pore volume correlate well with the surface area, for example (Table 6). MultiPoint BET and Total pore volume $r = 0.9744$. Langmuir surface area and Total pore volume $r = 0.9765$ (Fig. 5 (b)). Accordingly, similar patterns are observed for the pore volume (Fig. 6). It should also be noted that the maximum volume of micropores according to the t-method in BSB700-1 h and, accordingly, a clear increase in volume with temperature for the BJH, DH, t-method, DR methods is not observed, indicating that the appearance of pores does not lead to a significant increase in the volume of voids.

The study reveals that the pyrolysis temperature increases. the average pore size of the biochar material decreases significantly (Table 7**).** This decrease is indicative of the development of a highly microporous structure, a characteristic that plays a crucial role in the material's adsorption properties. At elevated temperatures, the thermal decomposition of organic material leads to the volatilization of smaller molecular compounds, resulting in the collapse or narrowing of mesopores and macropores. Consequently, the remaining structure exhibits an increased proportion of micropores, which are defined by their pore diameters being less than 2 nanometers. These micropores are particularly effective in absorbing and retaining small molecules, such as nitrogen, due to

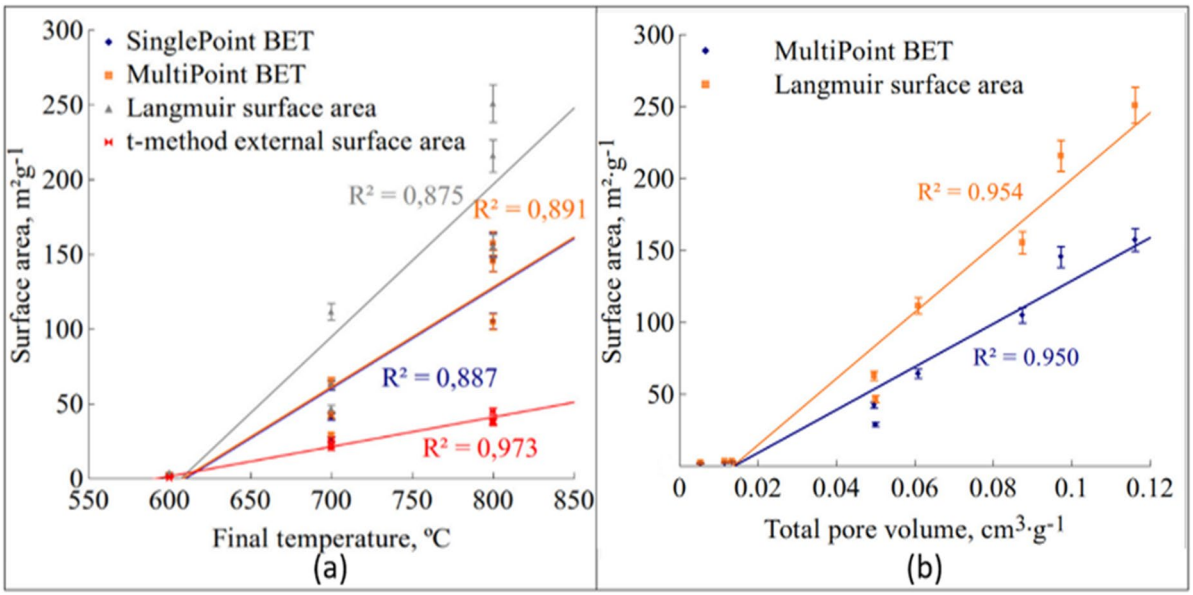

Fig. 5. (**a**) Correlation between surface area and final heating temperature, (**b**) correlation between surface area and total pore volume.

Pore volume calculation method, $cm^3 \cdot g^{-1}$								
Sample	Total pore volume	BJH ads\des. $\cdot 10^{-3}$	DH ads\des. $\cdot 10^{-3}$	t-method (micro)	DR (micro)	HK (micro)	SF (micro)	DFT
BSB600-1 h	0.01156	3.541/6.857	10.47/9.29	0.01047	0.00929	0.00152	0.002083	0.001068
BSB600-2 h	0.01339	4.532/6.501	12.49/10.09	0.01249	0.01009	0.00183	0.002492	0.001132
BSB600-3 h	0.00524	4.53/3.72	4.368/3.59	0.004368	0.00359	0.001591	0.001624	0.0008898
BSB700-1 h	0.04998	50.45/5.112	49.11/4.98	0.04911	0.00498	0.02255	0.03362	0.01003
BSB700-2 h	0.0496	25.76/4.516	36.2/10.88	0.0362	0.01088	0.02238	0.03447	0.01791
BSB700-3 h	0.06088	40.53/8.099	39.43/7.936	0.03943	0.007936	0.03385	0.0545	0.02726
BSB800-1 h	0.08743	45.61/7.739	44.36/7.663	0.04436	0.007663	0.05176	0.07454	0.04663
BSB800-2 h	0.09725	29.44/5.247	28.63/5.205	0.02863	0.005205	0.06755	0.09587	0.06861
BSB800-3 h	0.1162	30.15/8.169	43.37/15.96	0.04337	0.01596	0.07034	0.1506	0.071

Table 6. Pore volume characteristics of pyrolyzed pellets.

their high surface area and the specific interactions between the pore walls and the adsorbed molecules. This behavior is important for applications where the controlled retention and release of nitrogen are critical, such as in soil amendments and fertilizer formulations. The microporous architecture also enhances the material's capacity for selective adsorption, which can be advantageous in environmental applications, including the sequestration of greenhouse gases like nitrogen-based compounds. These findings underscore the necessity of optimizing pyrolysis conditions to tailor pore size distribution for specific functional applications.

Although the observed type IV isotherms with hysteresis loops are characteristic of mesoporous structures that can facilitate multilayer adsorption, this study focused primarily on single-layer surface area estimation using the BET model. Therefore, multilayer adsorption mechanisms were not explicitly analyzed. This represents a limitation of the current work and offers direction for future investigation using models such as BJH or DFT for more detailed pore structure analysis (Fig. 7) shows the dependence of total pore volume on biochar residence time and final heating temperature and the dependence of surface area on residence time and final heating temperature.

The process of biomass carbonization in an inert atmosphere affects the specific surface area of the product by changing the pore structure. As volatile products are released, hollow porous structures are formed, which significantly increases the specific surface area. As can be seen from the SEM micrographs, the formation of a pronounced porous structure is observed with increasing pyrolysis temperature (Fig. 8). Morphological studies showed the heterogeneity of the pellets. Biomass residues were visible on a slice of pellets, BSB600-3 h pellets were denser and more homogeneous, BSB800-3 h pellets had a more porous structure with a compacted pore system compared to BSB600-3 h and BSB700-3 h pellets as confirmed by BET studies.

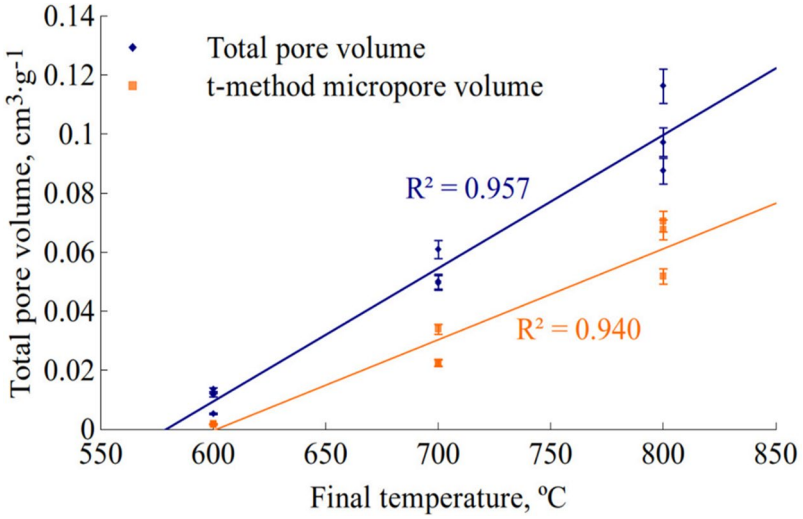

Fig. 6. Correlation between total pore volume and final pyrolysis temperature.

Pore size calculation method. average pore diameter, nm								
Sample	**Aver. pore diam.**	**BJH ads / des**	**DH ads/des**	**DR (micro)**	**DA**	**HK**	**SF**	**DFT**
BSB600-1 h	18.9	4.053 / 4.009	4.053 / 4.009	4.053	4.009	2.613	1.8	0.7925
BSB600-2 h	20.2	3.226 / 4.011	3.226 / 4.011	3.226	4.011	2.701	1.8	0.7325
BSB600-3 h	11.0	3.48 / 4.003	3.48 / 4.003	3.48	4.003	2.26	1.8	0.3675
BSB700-1 h	6.9	2.991 / 4.008	2.991 / 4.008	2.991	4.008	3.723	2.2	1.257
BSB700-2 h	4.7	2.991 / 4.014	2.991 / 4.014	2.991	4.014	2.95	2.22	1.072
BSB700-3 h	3.8	3.221 / 3.435	3.221 / 3.435	3.221	3.435	3.613	2.66	1.257
BSB800-1 h	3.3	2.989 / 4.013	2.989 / 4.013	2.989	4.013	2.423	1.96	0.3675
BSB800-2 h	2.7	2.99 / 4.023	2.99 / 4.023	2.99	4.023	2.481	1.94	0.3675
BSB800-3 h	2.9	2.99 / 4.018	2.99 / 4.018	2.99	4.018	3.695	2.18	1.077

Table 7. Pore size characteristics of pyrolyzed pellets based on different analytical methods.

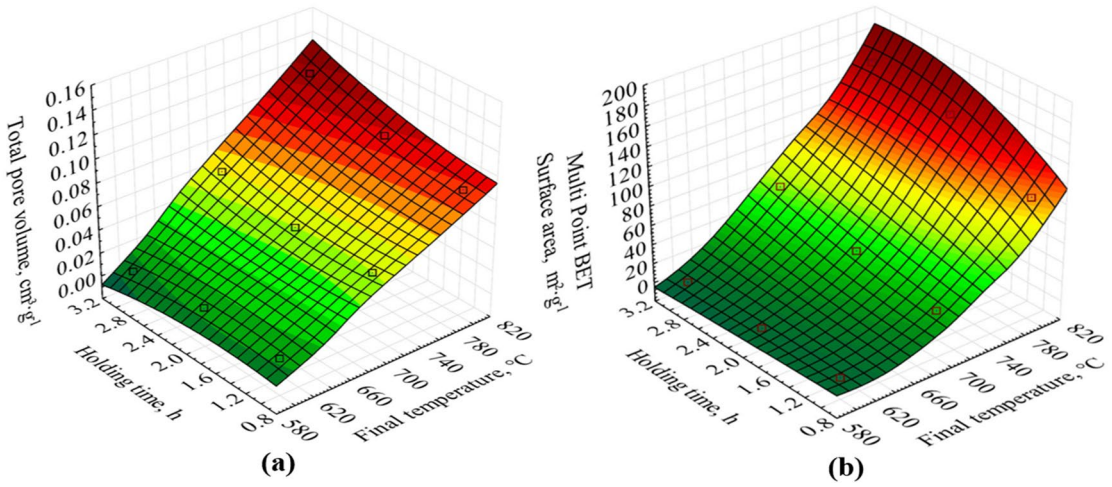

Fig. 7. (**a**) Dependence of total pore volume on holding time and final heating temperature, (**b**) dependence of surface area on holding time and final temperature.

Table 8 shows that slow pyrolysis alone produces biochar with low surface areas and pore volumes, whereas chemical or steam activation can increase S_{BET} to > 2000 $m^2 \cdot g^{-1}$ and V_{tot} to > 1 $cm^3 \cdot g^{-1}$.

Our barley straw–bran pellets followed the typical trend: biochar at 600 °C remained weakly porous (S_{BET} ≈ 2–3 $m^2 \cdot g^{-1}$), while raising the temperature to 700–800 °C progressively increased surface area to 64–157 $m^2 \cdot g^{-1}$ and pore volume to ~ 0.12 $cm^3 \cdot g^{-1}$. These values, however, are far below those achieved after chemical or steam

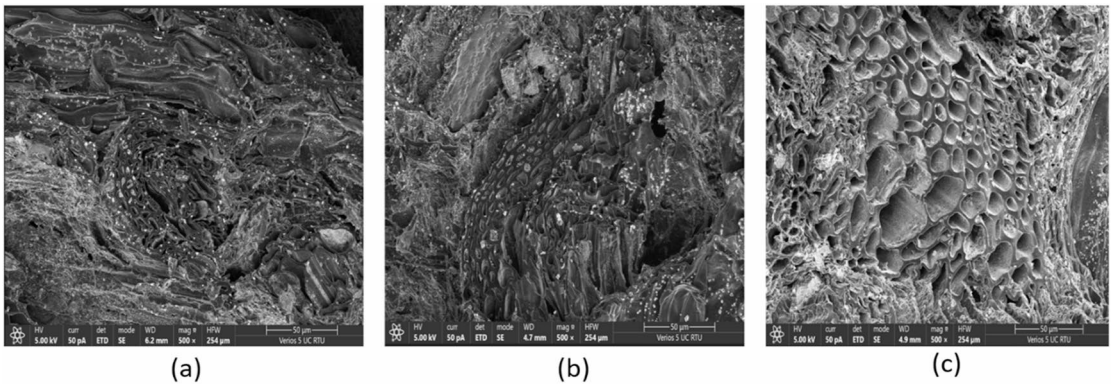

Fig. 8. Pellets morphology pyrolyzed at BSB600-3 h (**a**), at BSB700-3 h (**b**) and BSB800-3 h (**c**).

Feedstock	Pyrolysis temp, °C	Yield wt %	t, h	Heat. rate, °C·min^{-1}	Activat	Total pore volume cm^3·g^{-1}	S_{BET}, m^2·g^{-1}	Ref.
Corn stover	60–600	-	-	-	-	-	293–527	[15]
Walnut shell	400	-	1	10	-	0.078	74.06	[11]
Walnut shell	500	-	1	10	-	0.150	128.52	
Walnut shell	600	-	1	10	-	0.296	488.89	
Walnut shell	700	-	1	10	-	0.695	737.98	
Peanut shell	600	-	0.5	-	K_2CO_3	0.211	502.23	[16]
Peanut shell	600	-	0.5	-	K_2CO_3	0.320	750.16	
Peanut shell	600	-	0.5	-	K_2CO_3	0.433	1087.92	
Pine sawdust	850	10.01	1	5	KOH	1.46	2864.5	[17]
Pine sawdust	600	14.6	1	5	KOH	1.09	2437,2	
Pine sawdust	850	19.3	1	5	$ZnCl_2$	0.26	471.4	
Rapeseed husk	200	47.14	0.5	5	-	-	-	[18]
Orange peel	200	61.60	6	-	HCl	0.010	7.75	[19]
Orange peel	400	30.00	6	-	HCl	0.010	42.4	
Orange peel	700	22.20	6	-	HCl	0.035	201	
Wheat straw	450	-	4	10	-	0.048	45.05	[20]
Wheat straw	550	-	4	10	-	0,294	140.54	
Wheat straw	650	-	4	10	-	0.333	110.87	
Wheat straw	750	-	4	10	-	0.306	139.78	
Wheat straw	850	-	4	10	-	0.259	158.42	
Food waste	600	30.9	4	5	-	-	1.36	[21]
Food waste + wooden sawdust	600	35.4	4	5	-	-	1.83	
Barley straw	600	34.01	1	5	0.01156	2.446	Barley straw	Research results
Barley straw	600	33.55	2	5	0.01339	2.651	Barley straw	
Barley straw	600	33.00	3	5	0.005237	1.905	Barley straw	
Barley straw	700	30.78	1	5	0.04998	29.08	Barley straw	
Barley straw	700	31.31	2	5	0.0496	42.6	Barley straw	
Barley straw	700	31.30	3	5	0.06088	64.39	Barley straw	
Barley straw	800	30.50	1	5	0.08743	104.9	Barley straw	
Barley straw	800	30.20	2	5	0.09725	145.5	Barley straw	
Barley straw	800	30.08	3	5	0.1162	157.3	Barley straw	

Table 8. Comparative summary of pyrolysed biomass characteristics and experimental outcomes.

activation, confirming the need for subsequent activation to obtain high - performance sorbents. Future work will therefore include steam activation of the produced biochar to further enhance their porosity and adsorption capacity for wastewater treatment applications.

Data processing was performed with a Microsoft Excel for Windows 2013 program package (ANOVA) using a single-factor variance analysis with 2 repetitions. The calculation was performed separately for each indicator (LSD 0.05).

Sample	Relative to BSB600-1 (total pore volume)	Relative to BSB600-1 (S_{BET})
BSB600-1 h	0	0.00
BSB600-2 h	0.00183	0.21
BSB600-3 h	-0.00632	-0.54
BSB700-1 h	0.03842	26.63
BSB700-2 h	0.03804	40.15
BSB700-3 h	0.04932	61.94
BSB800-1 h	0.07587	102.45
BSB800-2 h	0.08569	143.05
BSB800-3 h	0.10464	154.85

Table 9. Analysis of variance.

The ANOVA results indicate a statistically significant increase in both total pore volume and specific surface area (BET) with increasing pyrolysis temperature from 600 °C to 800 °C. The most pronounced differences were observed between samples BSB600 and BSB800, with SBET rising by up to 154.85% and total pore volume increasing by 0.10464 $cm^3 \cdot g^{-1}$ (Table 9). These findings confirm that pyrolysis temperature is a key factor influencing the development of the porous structure in biochar.

Lower temperatures (400–600 °C) tend to be more energy efficient. For instance, a study observed that increasing the pyrolysis temperature from 400 °C to 600 °C boosted energy efficiency from 43.51% to 59.43% [39]. Higher Temperatures (600–800 °C) enhance the quality of biochar but may also increase energy demands. Research indicates that the heat required for pyrolysis varies with temperature and feedstock characteristics. For example, the energy needed for pyrolysis at 823 K (approximately 550 °C) ranged from 0.55 $MJ \cdot kg^{-1}$ in a fixed-bed reactor to 2.30 $MJ \cdot kg^{-1}$ in a screw conveyor pyrolysis reactor[40].

The scalability and environmental impact of biochar production are closely tied to the energy demands associated with pyrolysis temperature. Lower pyrolysis temperatures typically result in higher biochar yields and reduced energy consumption, thereby improving overall energy efficiency. In contrast, higher temperatures promote the formation of volatile products such as syngas and bio-oil at the expense of solid biochar. While this shift in product distribution can be advantageous for energy recovery applications, it may not align with objectives prioritizing biochar production for soil amendment, carbon sequestration, or sorbent use. Additionally, the elevated energy input required at higher pyrolysis temperatures can contribute to a greater carbon footprint, unless offset by capturing and utilizing the energy-rich syngas produced during the process. Therefore, the selection of pyrolysis temperature must balance energy efficiency, desired product yield, and environmental considerations. Operating at moderate temperatures, such as around 600 °C, may provide an optimal compromise by producing structurally suitable biochar while maintaining energy efficiency and minimizing negative environmental impacts.

While this study presents insights into the production of biochar from compacted agricultural residues, several limitations should be acknowledged. Much of the work - including pyrolysis, surface area analysis, and thermal characterization - was conducted at the laboratory scale, which may limit the direct transferability of results to industrial applications due to differences in heat distribution, reactor design, and energy efficiency. However, it is important to note that the granulation process was carried out using an industrial-grade pelletizer, ensuring that the mechanical properties and pellet formation reflect commercially viable conditions. Another limitation is the absence of experimental sorption performance tests (e.g. for heavy metals, nutrients, or volatile organics), which are necessary to confirm the functional efficacy of the biochar for specific environmental applications. Furthermore, the study was limited to a single type of biomass blend-barley straw with barley bran - restricting the generalization of the findings to other agricultural residues. Future work should expand the feedstock variety, include pilot-scale pyrolysis trials, and incorporate direct application testing to comprehensively evaluate the biochar's performance and scalability.

Limitations of the study

FTIR spectroscopy was not performed in this study, which prioritized textural and morphological characterization; as a limitation, future work will integrate ATR-/TG-FTIR to elucidate the evolution of surface functional groups across pyrolysis temperatures and residence times.

Conclusions

This study demonstrates the feasibility of producing biochar with tailored structural properties from mechanically compacted agricultural residues, specifically barley straw and bran, through controlled slow pyrolysis. In contrast to conventional methods utilizing bulk biomass, the use of pre-formed granules introduces a process-relevant advancement with implications for industrial scalability. The experimental results reveal that elevated pyrolysis temperatures and extended residence times significantly enhance the development of microporous and mesoporous structures, with samples BSB800-2 h and BSB800-3 h exhibiting the highest surface area and pore characteristics among the tested samples. Notably, samples BSB800-1 h, BSB700-2 h, and BSB700-3 h also display promising characteristics and warrant further investigation, particularly with respect to post-pyrolysis activation processes aimed at developing low-cost sorbents for environmental applications. Nonetheless, the study has certain limitations. The pyrolysis experiments and material characterization were conducted

at laboratory scale, which may not fully reflect the performance of the process under industrial conditions. Furthermore, sorption efficiency was inferred from physicochemical parameters without direct performance testing, and the investigation was limited to a single type of biomass-binder composition. However, the use of an industrial-grade granulator enhances the practical relevance of the findings and supports their potential transferability to commercial-scale systems. Future work should prioritize pilot-scale validation of the pyrolysis process, along with application-specific sorption experiments in real environmental matrices. Expanding the range of feedstocks and binder systems will further elucidate the adaptability of the method across different agricultural waste streams. In addition, life cycle assessment and techno-economic analysis are necessary to evaluate the environmental sustainability and economic viability of the approach. Finally, this research is aligned with the European Union's strategic vision for biorefinery development, which advocates for the integrated conversion of biomass into fuels, chemicals, and high-value materials. The incorporation of compacted-biomass pyrolysis into such systems represents a promising pathway toward resource-efficient, low-carbon, and circular bioeconomy solutions. Future research will focus on chemical activation of pelletized biochar and subsequent evaluation of its adsorption performance in water treatment applications.

Data availability

The data and materials presented in this study are available on request from the corresponding author.

Received: 6 May 2025; Accepted: 30 October 2025
Published online: 28 November 2025

References

1. Koide, R., Yamamoto, H., Nansai, K. & Murakami, S. Agent-based model for assessment of multiple circular economy strategies: quantifying product-service diffusion, circularity, and sustainability. *Resour. Conserv. Recycl.* **199**, 107216. https://doi.org/10.1016/j.resconrec.2023.107216 (2023).
2. Tong, W., Cai, Z., Liu, Q., Ren, S. & Kong, M. Effect of pyrolysis temperature on bamboo Char combustion: Reactivity, kinetics and thermodynamics. *Energy* **211**, 118736. https://doi.org/10.1016/j.energy.2020.118736 (2020).
3. Vincevica-Gaile, Z. et al. Selected residual biomass valorization into pellets as a circular economy-supported end-of-waste. *Clean. Mater.* **15**, 100295. https://doi.org/10.1016/j.clema.2025.100295 (2025).
4. Irtiseva, K. et al. Application of granular biocomposites based on homogenised peat for absorption of oil products. *Mater* **15**, 41306. https://doi.org/10.3390/ma15041306 (2022).
5. Shishkin, A. et al. Influence of waste glass in the foaming process of open cell porous ceramics as filtration media for industrial wastewater. *J. Clean. Prod.* **282**, 124546. https://doi.org/10.1016/j.jclepro.2020.124546 (2021).
6. Shishkin, A., Grigorjeva, L., Ghaffari, H., Goel, J. & Ozolins, J. Influence of glass additions on illitic clay ceramics. *Mater* **13**, 596. https://doi.org/10.3390/ma13030596 (2020).
7. Lauberts, M., Mierina, I., Pals, M., Latheef, M. A. A. & Shishkin, A. Spent coffee grounds valorization in biorefinery context to obtain valuable products using different extraction approaches and solvents. *Plants* **12**, 2345. https://doi.org/10.3390/plants12010030 (2023).
8. Farhat-Bensalah, A., Haddad, I., Houas, H., Al-Hammadi, A. & Al-Sabagh, A. Activated carbon design from sludge to remove red Scarlet Nylosan F3GL in aqueous solution. *Key Eng. Mater.* **762**, 87–92. https://doi.org/10.4028/www.scientific.net/KEM.762.87 (2018).
9. Reka, A. A. et al. Diatomaceous earth: Characterization, thermal modification, and application. *Open. Chem.* **19**, 451–461. https://doi.org/10.1515/chem-2020-0049 (2021).
10. Khan, T. A. et al. Hydrothermal carbonization of lignocellulosic biomass for carbon-rich material preparation: A review. *Biomass Bioenergy*. **130**, 105384. https://doi.org/10.1016/j.biombioe.2019.105384 (2019).
11. Xu, H., Han, Y., Wang, G., Deng, P. & Feng, L. Walnut shell Biochar based sorptive remediation of estrogens polluted simulated wastewater: Characterization, adsorption mechanism and degradation by persistent free radicals. *Environ. Technol. Innov.* **28**, 102870. https://doi.org/10.1016/j.eti.2022.102870 (2022).
12. Wang, Y., Wang, S., Ling, X., Xie, T. & Cao, J. Activated carbon derived from waste Tangerine seed for the high-performance adsorption of carbamate pesticides from water and plant. *Bioresour Technol.* **316**, 123929. https://doi.org/10.1016/j.biortech.2020.123929 (2020).
13. Greish, A. A. et al. Adsorption of phenol and 2,4-dichlorophenol on carbon-containing sorbent produced from sugar cane Bagasse. *Mendeleev Commun.* **31**, 121–122. https://doi.org/10.1016/j.mencom.2021.01.038 (2021).
14. Huang, X. et al. Combined resource utilization of Ash from biomass power generation and wheat straw biochar for soil remediation. *Appl. Soil. Ecol.* **191**, 105150. https://doi.org/10.1016/j.apsoil.2023.105150 (2023).
15. Nguyen, T. T. V. et al. Valorization of agriculture waste biomass as biochar: as first-rate biosorbent for remediation of contaminated soil. *Chemosphere* **307**, 135834. https://doi.org/10.1016/j.chemosphere.2022.135834 (2022).
16. Xu, Y. et al. Enhancing CO_2 capture with K_2CO_3-activated carbon derived from peanut shell. *Biomass Bioenerg.* **183**, 107148. https://doi.org/10.1016/j.biombioe.2024.107148 (2024).
17. Pimentel, C. H., Díaz-Fernández, L., Gómez-Díaz, D., Freire, M. S. & González-Álvarez, J. Separation of CO_2 using Biochar and KOH- and $ZnCl_2$-activated carbons derived from pine sawdust. *J. Environ. Chem. Eng.* **11** (6), 111378. https://doi.org/10.1016/j.jece.2023.111378 (2023).
18. Elaigwu, S. E. & Greenway, G. M. Microwave-assisted hydrothermal carbonization of rapeseed husk: A strategy for improving its solid fuel properties. *Fuel Process. Technol.* **149**, 305–312 (2016). https://doi.org/10.1016/j.fuproc.2016.04.030
19. Chen, B. & Chen, Z. Sorption of naphthalene and 1-naphthol by biochars of orange peels with different pyrolytic temperatures. *Chemosphere* **76**, 127–133. https://doi.org/10.1016/j.chemosphere.2009.02.004 (2009).
20. Xu, Y., Qu, G., Yan, Z., Wu, H. & Ning, P. Metal oxide–molten salt catalyzed pyrolysis: improving the energy conversion efficiency of wheat straw. *Process Saf. Environ. Prot.* **192**, 1051–1061. https://doi.org/10.1016/j.psep.2024.10.118 (2024).
21. Raček, J. et al. Biochar production from the pyrolysis of food waste: characterization and implications for its use. *Sustainable Chem. Pharm.* **37**, 101387. https://doi.org/10.1016/j.scp.2023.101387 (2024).
22. Gupta, N. K., Gupta, A., Ramteke, P., Sahoo, H. & Sengupta, A. Biosorption – a green method for the preconcentration of rare earth elements (REEs) from waste solutions: A review. *J. Mol. Liq.* **274**, 148–164. https://doi.org/10.1016/j.molliq.2018.10.134 (2019).
23. Lu, L. et al. Application of biochar-based materials in environmental remediation: from multi-level structures to specific devices. *Biochar* **2**, 421–444. https://doi.org/10.1007/s42773-020-00041-7 (2020).
24. Wang, B., Gao, B. & Fang, J. Recent advances in engineered biochar productions and applications. *Crit. Rev. Environ. Sci. Technol.* **47**, 2158–2207. https://doi.org/10.1080/10643389.2017.1418580 (2017).

25. Chen, W. H., Ong, H. C. & Bhaskar, T. Biomass processing for biofuels, bioenergy and chemicals. *Energies* (2020). https://doi.org/10.3390/books978-3-03928-910-3
26. Yadav, N. Pharmaceutical processing – A review on wet granulation technology. *Int. J. Pharmaceut. Front. Res.* **1**(1), 65–83 (2011). https://www.researchgate.net/publication/228453068_Pharmaceutical_Processing-A_Review_on_Wet_Granulation_Technology (Accessed: 2 October 2025).
27. Fan, R. et al. Sustainably transforming biomass into advanced carbon materials for solid-state supercapacitors: a review. *Chem. Commun.* **60**, 13219–13242. https://doi.org/10.1039/D4CC04762A (2024).
28. Sun, J. X., Xu, F., Sun, X. F., Xiao, B. & Sun, R. C. Physico-chemical and thermal characterization of cellulose from barley straw. *Polym. Degrad. Stab.* **88**, 521–531. https://doi.org/10.1016/j.polymdegradstab.2004.12.013 (2005).
29. Monforti, F., Bódis, K., Scarlat, N. & Dallemand, J. F. The possible contribution of agricultural crop residues to renewable energy targets in Europe: A spatially explicit study. *Renew. Sustain. Energy Rev.* **19**, 666–677. https://doi.org/10.1016/j.rser.2012.11.060 (2013).
30. Zhylina, M. et al. Granulation and pyrolysis of agricultural residues for an enhanced circular economy. *Results Eng.* **26**, 104919. https://doi.org/10.1016/j.rineng.2025.104919 (2025).
31. Irtiseva, K. et al. Processing of Latvian peat and waste coffee as a biocomposite material for the oil spill collection. *Agron. Res.* **22**, 146–156. https://doi.org/10.15159/AR.24.040 (2024).
32. Reza, M. S. et al. Investigation of thermochemical properties and pyrolysis of barley waste as a source for renewable energy. *Sustainability* **15**, 1643. https://doi.org/10.3390/su15021643 (2023).
33. Singh, H., Sapra, K. & Sidhu, B. S. Evaluation and characterization of different biomass residues through proximate & ultimate analysis and heating value. *Asian J. Eng. Appl. Technol.* **2** (2), 6–10. https://doi.org/10.51983/ajeat-2013.2.2.690 (2013).
34. Lazdovica, K., Liepina, L. & Kampars, V. Catalytic pyrolysis of wheat Bran for hydrocarbons production in the presence of zeolites and noble metals by using TGA-FTIR method. *Bioresour. Technol.* **207**, 126–133. https://doi.org/10.1016/j.biortech.2016.01.117 (2016).
35. Volperts, A. et al. Biomass based activated carbons for fuel cells. *Renew. Energy*. **141**, 40–45. https://doi.org/10.1016/j.renene.2019.04.002 (2019).
36. International Organization for Standardization (ISO). *ISO 9277:2010 — Determination of the Specific Surface Area of Solids by Gas Adsorption — BET Method* (ISO, 2010).
37. Belhachemi, M. & Addoun, F. Effect of heat treatment on the surface properties of activated carbons. *E-J. Chem.* **8** (S1), S1–S7. https://doi.org/10.1155/2011/649254 (2011).
38. Guo, Y. et al. Pore structure and fractal characteristic analysis of gasification-coke prepared at different high-temperature residence times. *ACS Omega*. **5**, 22226–22237. https://doi.org/10.1021/acsomega.0c02399 (2020).
39. Hasan, M. M., Rasul, M. G., Jahirul, M. I. & Mofijur, M. Fuelling the future: unleashing energy and exergy efficiency from municipal green waste pyrolysis. *Fuel* **357**, 129815. https://doi.org/10.1016/j.fuel.2023.129815 (2024).
40. Jerzak, W., Reinmöller, M. & Magdziarz, A. Estimation of the heat required for intermediate pyrolysis of biomass. *Clean Technol. Environ. Policy*. **24**, 3061–3075. https://doi.org/10.1007/s10098-022-02391-1 (2022).

Acknowledgements

This activity/work has been supported by the EU Recovery and Resilience Facility within the Project No 5.2.1.1.i.0/2/24/I/CFLA/003 "Implementation of consolidation and management changes at Riga Technical University, Liepaja University, Rezekne Academy of Technology, Latvian Maritime Academy and Liepaja Maritime College for the progress towards excellence in higher education, science and innovation" academic career doctoral grant (ID 1024).Access to the infrastructure and expertise of the BBCE—Baltic Biomaterials Centre of Excellence (European Union's Horizon 2020 research and innovation program under Grant Agreement No. 857287).

Author contributions

Maryna Zhylina: Conceptualization, Methodology, Investigation, Data curation, writing – original draft, Denis Miroshnichenko: Methodology and Supervision, Andrii Melnykov: Testing and characterisation, Valentina Stepanova: Testing, Kristine Lazdovica: writing – original draft, Reviewing and editing, Vjaceslavs Zemcenkovs: Organising raw materials, Vita Sterna: Reviewing and editing, Jurijs Ozolins: Review, editing and supervision.

Declarations

Competing interests

The authors declare no competing interests.

Additional information

Correspondence and requests for materials should be addressed to D.M.

Reprints and permissions information is available at www.nature.com/reprints.

Publisher's note Springer Nature remains neutral with regard to jurisdictional claims in published maps and institutional affiliations.